LQG/LTR ROBUST ACTIVE SUSPENSION CONTROL APPLIED ON A NONLINEAR HALF-VEHICLE MODEL

Murilo F. Falleiros*, Diego Colón*

*Departamento de Engenharia de Telecomunicações e Controle (PTC)
Escola Politécnica da Universidade de São Paulo
Av. Prof. Luciano Gualberto, travessa 3, nº 158
São Paulo, SP, Brasil

Emails: murilofregonesi@hotmail.com, diego@lac.usp.br

Abstract— This paper presents a linear LQG/LTR robust controller design for a half-vehicle model active suspension system with nonlinear electromagnetic actuators. The control scheme aims ride comfort improvement whilst guaranteeing suspension travel and actuators force limits. The actuators forces are labeled as the control inputs of the system and the wheels position are the non-controllable inputs. System robustness is based on parametric uncertainties, which are the vehicle mass, varying with the number of passengers, and the spring stiffness coefficient. Disturbance bump signals are imposed to the wheels in order to evaluate final suspension system behavior and enhance control system design. A discussion about the LQG/LTR controller behavior when applied to a nonlinear plant is performed as well.

Keywords— LQG/LTR, Robust control, Active suspension, Half-vehicle model.

Resumo— Este trabalho apresenta o desenvolvimento de um controlador robusto linear LQG/LTR para um modelo de suspensão ativa em meio veículo com atuadores eletromagnéticos não lineares. O esquema de controle visa melhorias no conforto de condução enquanto garante os limites de deslocamento da suspensão e força dos atuadores. As forças dos atuadores são designadas como as entradas de controle do sistema e a posição das rodas são as entradas não controláveis. A robustez do sistema é baseada em incertezas paramétricas, sendo elas a massa do veículo, variando com o número de passageiros, e o coeficiente de rigidez da mola. Distúrbios tipo lombada são impostos às rodas com o intuito de avaliar o comportamento final do sistema de suspensão e desenvolver o sistema de controle. Uma discussão sobre o comportamento do controlador LQG/LTR quando aplicado à uma planta não linear é feita também.

Palavras-chave— LQG/LTR, Controle robusto, Suspensão ativa, Modelo de meio veículo.

1 Introduction

Automotive industry has been increasingly charged for improvements in handling performance and ride comfort, besides all safety and environmental legal requirements. On top of that, many studies of active suspension systems has been performed in the last decades proposing different approaches for the systems control, such as nonlinear (Huang and Lin, 2004), optimal (van der Sande, 2011), robust (Kong et al., 2015) and adaptative (Alleyne and Hedrick, 1995) methods, and modifications on suspension structure, with hydraulic (Alleyne and Hedrick, 1995) and electromagnetic (van der Sande, 2011) actuators.

Assessment of users perception of comfort and exposure limits for healthy preservation is often based on ISO 2631:1997 (ISO, 1997), for instance as presented in dos Santos (2010) and van der Sande (2011), which is basically a guide for evaluation of human exposure to whole-body vibration.

The active suspension control system developed in this paper, based on the application of the LQG/LTR robust procedure, aims ride comfort improvement whilst guaranteeing the limits of suspensions travel and Root-Mean-Square (RMS) actuators force. Therefore, vehicle handling performance is out of active system response evaluation criteria. Robustness of the controller is based on parametric uncertainties which were considered in the model, being these the vehicle mass, which varies according to the number of passengers, and the spring stiffness coefficient.

A half-vehicle model is presented in order to verify the closed loop active system response, which includes electromagnetic actuators nonlinearities. The actuators forces are labeled as the control inputs of the system and the wheels positions are the disturbances, or non-controllable inputs. Disturbance bump signals are imposed to the wheels in order to compare passive and active systems responses and to enhance control design.

2 Plant structuring

2.1 System modeling

In Figure 1 the linear four degrees of freedom (4-DOF), where the sprung mass includes 2-DOF on vertical and pitching movements while the unsprung masses include more 2-DOF on both vertical displacements, half-vehicle model is presented, which carries an active suspension system.

In the half-vehicle model, frontal and rear unsprung masses weight and position are represented by m_f and m_r, and Z_{tf} and Z_{tr}, respectively. The wheels have their stiffness coefficients labeled as k_{tf} and k_{tr} with negligible damping coefficient and

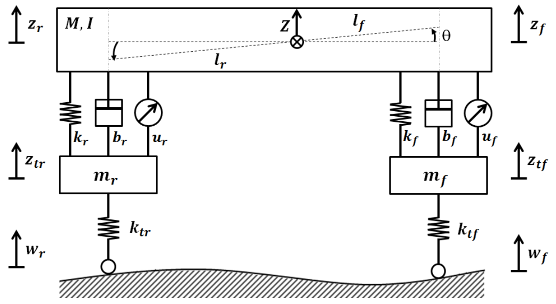

Figure 1: Half-vehicle model.

are in constant contact with the ground of frontal and rear highness w_f and w_r. Lastly the two suspension systems, located between the sprung mass M at Z_f and Z_r positions and the unsprung masses, are divided in a passive portion and an active one. The passive suspension system is modeled by stiffness coefficients k_f and k_r (suspension springs) and damping coefficients b_f and b_r (suspension dampers), while the active portion is defined by electromagnetic generated forces u_f and u_r. The chassis, or sprung mass, has moment of inertia I, pitch angle θ, frontal and rear body portions (distance between the gravity center and suspension link) l_f and l_r and gravity center vertically positioned at Z.

Equation (1) introduces the sprung mass dynamics with second order differential equations.

$$M\ddot{Z} = F_f + F_r \tag{1a}$$

$$I\ddot{\theta} = l_f F_f - l_r F_r \tag{1b}$$

Where,

$$F_f = u_f - k_f(z_f - z_{tf}) - b_f(\dot{z}_f - \dot{z}_{tf}) \tag{2a}$$

$$F_r = u_r - k_r(z_r - z_{tr}) - b_r(\dot{z}_r - \dot{z}_{tr}) \tag{2b}$$

The electromagnetic actuators generated forces u_f and u_r are defined by Equation (3), which are divided in a passive portion, resulted from the suspension velocities v_f and v_r, and an active portion dependent on actuators current amplitude $\hat{i}_f$ and $\hat{i}_r$ (van der Sande, 2011).

$$u_{af} = 115\hat{i}_f - 1341\ arctan(0.985 v_f) \tag{3a}$$

$$u_{ar} = 115\hat{i}_r - 1341\ arctan(0.985 v_r) \tag{3b}$$

Actuator introduced before is a tubular slotted three-phase permanent magnet actuator (TPMA), capable of delivering large amounts of force with little power consumption when compared with a hydraulic system. Active force may be approximated as a linear function of current, as shown in Equation (3), while passive damping force is a result of the implemented stator aluminum rings, which provide Eddy's current damping force according to the suspension velocity.

The sprung mass vertical positions, into the suspension systems fixation points, are described in Equation (4).

$$z_f = Z + l_f\theta \tag{4a}$$

$$z_r = Z - l_r\theta \tag{4b}$$

Lastly, the unsprung masses dynamics are presented in Equation (5).

$$m_f\ddot{z_{tf}} = -F_f - k_{tf}(z_{tf} - w_f) \tag{5a}$$

$$m_r\ddot{z_{tr}} = -F_r - k_{tr}(z_{tr} - w_r) \tag{5b}$$

To construct a state-space description of the model presented before, let us define $x(t) = [x_1\ x_2\ x_3\ x_4\ x_5\ x_6\ x_7\ x_8]^T$ as the states vector, $u_a(t) = [u_f\ u_r]^T$ as the control inputs vector, $w(t) = [w_f\ w_r]^T$ as the disturbance (non-controllable) inputs vector, $y(t) = [x_1\ x_7]^T$ as the output vector. Where $x_1 = Z$, $x_2 = \dot{Z}$, $x_3 = z_{tf}$, $x_4 = \dot{z}_{tf}$, $x_5 = z_{tr}$, $x_6 = \dot{z}_{tr}$, $x_7 = \theta$ and $x_8 = \dot{\theta}$.

The half-vehicle plant of Figure 1 state-space description is exhibited in Equation (6).

$$\dot{x}_p(t) = A_p x(t) + B_{p1}u_a(t) + B_{p2}w(t) \tag{6a}$$

$$y_p(t) = C_p x(t) \tag{6b}$$

Where the input matrix B_p was divided in two parts, one for control inputs and other to the non-controllable, or disturbance, inputs.

2.2 *System analysis*

As the LQG/LTR robust procedure requires a linear time invariant (LTI) and square defined system, Equation (6) must be modified to works as plant in controller's design. Therefore, the influences of $u_a(t)$ and $w(t)$ are separated, what is possible once the plant state-space description is linear, thus, two new models are constructed to represent the whole system. Dividing the model in two parts, the first one is based on input matrix B_{p1} of control inputs, which is hereafter considered as nominal plant to controller's development. Disregarding the disturbances on the system, the new state space description for the plant is presented in Equation (7).

$$\dot{x}_p(t) = A_p x(t) + B_{p1}u_a(t) \tag{7a}$$

$$y_p(t) = C_p x(t) \tag{7b}$$

The second part of the plant is restricted for the non-controllable inputs matrix B_{p2}, whose influence is now determined as disturbance input to the half-vehicle system. To a non-actuated system, the state space description for disturbance inputs is described in Equation (8).

$$\dot{x}_p(t) = A_p x(t) + B_{p2}w(t) \tag{8a}$$

$$y_p(t) = C_p x(t) \tag{8b}$$

Besides system stability robustness guarantee, the final control project must obey the following performance robustness requirements: *reference signal tracking*, *disturbance rejection* and *measurement error rejection*, which are visually evaluated in frequency domain, whose angular frequency ranges are determined through the new state-space descriptions. Logically, the plant representation of Equation (7) is the base for reference signal tracking whose singular values plots are presented in Figure 2.

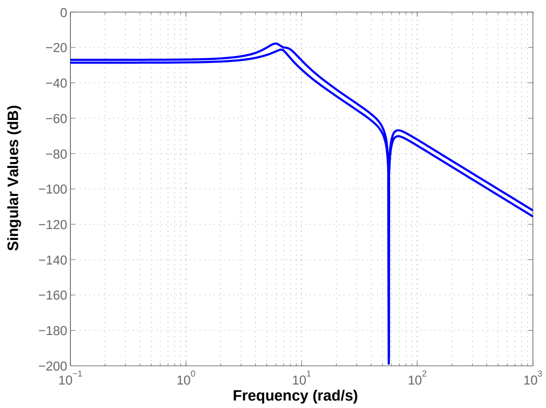

Figure 2: Singular values to controllable inputs.

Considering the system response to controllable inputs, there is no great influence after 10 rad/s, thus, the bandwidth for reference signal tracking evaluation may be defined as: $\Omega_r = \{\omega \in R : \omega \leq 10\ rad/s\}$.

Analyzing the drastic fall of the singular values at $56.7rad/s$ in Figure 2, if we evaluate the transmission zeros of the controllable plant described in Equation (7), the following values are found: $s_{1,2} = s_{3,4} = 0 \pm 56.75i$. As a *transmission zero* is a complex value of s which leads a MIMO system output to zero, or $y(t) = 0$, it explains well the phenomena observed in the above singular values plot.

Proceeding, the disturbance influence of Equation (8) is the base for the disturbance rejection requirement, which singular values plots are presented in Figure 3. Here the non-controllable inputs are previously multiplied per 1000 to make a graphical analysis easier.

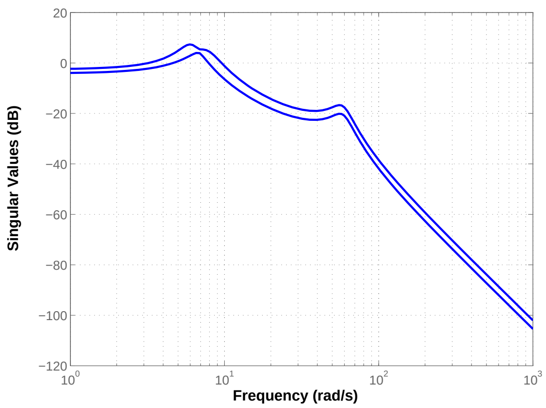

Figure 3: Singular values to disturbance inputs.

As did for the control inputs, now regarding the system response to disturbance inputs, it has a considerable influence up to 10 rad/s as well, resulting in a bandwidth for disturbance rejection evaluation of: $\Omega_d = \{\omega \in R : \omega \leq 10\ rad/s\}$. Regarding measurement error rejection criteria, reasonable values were defined to represent a sensor sampling rate in a possible system implementation as: $\Omega_n = \{\omega \in R : \omega \geq 500\ rad/s\}$.

Finalizing performance barriers design, tolerance limits to tracking error α_r, disturbance α_d and measurement error α_n must be delimited. As detailed in section 4, nonlinearities of the suspension actuator influenced the vehicle behavior and controller's response, being necessary to increase tolerances until it present acceptable system responses. The final values reached were $\alpha_r = 0.6$, $\alpha_d = 0.7$, and $\alpha_n = 0.1$.

Error modeling is performed through two parameters variation: sprung mass M, which varies from $535kg$ to $625kg$ representing the passengers number uncertainty, and suspension stiffness coefficients k_f and k_r, which varies from $15131N/m$ to $18493N/m$ representing 10% of parameter error.

3 Controller Design

In this section the LQG/LTR technique is applied to design an adequate control system represented by the closed-loop system of Figure 4 (Cruz, 1996).

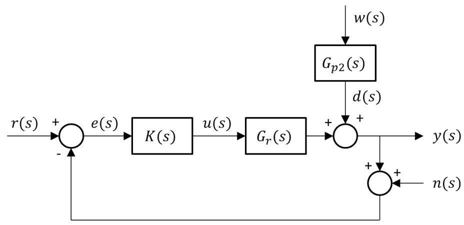

Figure 4: Block diagram for closed-loop system.

Where, $r(s)$ is the reference signal, $e(s)$ is the error signal, $u(s)$ is the control signal, $d(s)$ is the disturbance signal, $y(s)$ is the output signal, and $n(s)$ is the measurement error. Also $G_r(s)$ represents the real system transfer function matrix, which to nominal values of parametric uncertainties is defined as the frequency response matrix $G_p(j\omega)$, exhibited in Equation (9).

$$G_p(j\omega) = C_p(j\omega I - A_p)^{-1}B_{p1} \tag{9}$$

Additionally, $G_{p2}(j\omega)$ represents the disturbance frequency response matrix that is described in Equation (10).

$$G_{p2}(j\omega) = C_p(j\omega I - A_p)^{-1}B_{p2} \tag{10}$$

Here measurement error signal $n(s)$ is not considered, also the reference signal $r(s)$ is equal to zero. To the pairs (A_p, C_p) observable and

(A_p, B_{p1}) controllable, the model-based compensator structure adopted in LQG/LTR methodology to $K(s)$ is presented in Figure 5.

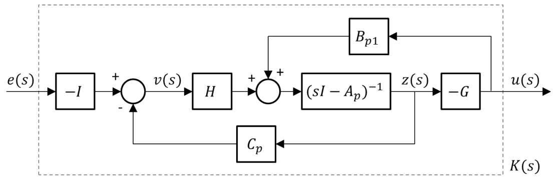

Figure 5: Controller block diagram.

The state feedback gain matrix G and the Kalman filter gain matrix H are the free controller parameters which must be well-chosen in order to achieve the project requirements (Cruz, 1996). To achieve this, firstly the target loop $G_{KF}(s)$ behavior is defined through the variation of μ and L to satisfy the stability and performance requirements. To $\mu \ll 1$, the target loop singular values description may be approximated by Equation (11) in both in low and high frequencies.

$$\sigma_i[G_{KF}(j\omega)] \simeq \frac{1}{\sqrt{\mu}}\sigma_i[C_p(j\omega I - A_p)^{-1}L] \quad (11)$$

Due to plant nonlinearities, neglected in control design, the isolated selection of μ and L often result in non-desirable system responses. Therefore, the graphical selection process was exchanged by an iterative process of simulation using μ, L and ρ to select the best combination whose final response was acceptable. The final parameters were: $\mu = 10^{-4}$, $\rho = 10^{-8}$, and $L = B_{1p}$.

After parameters selection, robustness stability and performance requirements must be verified. To accomplish that, the *reference tracking robustness condition*, the *disturbance rejection robustness condition*, the *measurement error rejection robustness condition* and the *stability robustness condition*, which are sequentially exhibited in Equation (12), must be respected.

$$\sigma_m[G_p(j\omega)K(j\omega)] \geq \frac{1}{\alpha_r}\frac{1}{1-e_M(\omega)}, \ (\omega \leq \omega_r) \quad (12a)$$

$$\sigma_m[G_p(j\omega)K(j\omega)] \geq \frac{1}{\alpha_d}\frac{1}{1-e_M(\omega)}, \ (\omega \leq \omega_d) \quad (12b)$$

$$\sigma_M[G_p(j\omega)K(j\omega)] \leq \frac{\alpha_n}{1+e_M(\omega)}, \ (\omega \geq \omega_n) \quad (12c)$$

$$\sigma_M[C_p(j\omega)] < \frac{1}{e_M(\omega)} \quad (12d)$$

In which $C_p(j\omega)$ is the plant closed-loop transfer function matrix and $e_M(\omega)$ is the maximum modeling error in multiplicative form defined in Equation (13), where the maximum value of $\varepsilon_M(s)$ is find varying $G_r(s)$ uncertainties within its bounds.

$$\varepsilon_M(s) = (G_r(s) - G_p(s))G_p^{-1}(s) \quad (13a)$$

$$||\varepsilon_M(j\omega)|| \leq e_M(\omega) \quad (13b)$$

Figure 6 presents the target loop approximated singular values (red line) and robustness performance and stability barriers (blue dashed lines) defined previously in order to verify robustness stability and performance requirements.

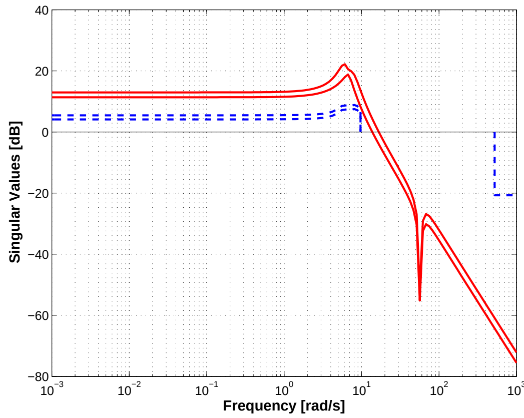

Figure 6: Approximated target loop singular values and performance barriers.

Barriers respected, hereafter the control problem is summarized as finding an adequate Kalman filter gain matrix H which satisfies the control prerequisites and, consequently, through the application of the Loop Transfer Recovery (LTR) procedure, the closed-loop response of 5 would attend the project requirements. The Kalman Filter matrix H is defined by Equation (14).

$$H = \frac{1}{\mu}\Sigma C_p' \quad (14)$$

Where Σ is found by solving the Algebraic Riccati equation (A.R.E) of Equation (15).

$$0 = A_p\Sigma + \Sigma A_p' + LL' - \frac{1}{\mu}\Sigma C_p' C_p \Sigma \quad (15)$$

Therefore, the target loop transfer function matrix $G_{KF}(j\omega)$, applied on LTR methodology, is described by Equation (16).

$$G_{KF}(j\omega) = C_p(j\omega I - A_p)^{-1}H \quad (16)$$

It is necessary that the closed-loop target loop singular values respect the robustness stability criteria defined in Equation (12). The diagram which proves robust stability condition for the target loop is presented in Figure 7, where the blue line represents the stability barrier and the red lines represent the closed-loop singular values.

Equation (17) defines the states feedback matrix G.

$$G = \frac{1}{\rho}B_{p1}' K \quad (17)$$

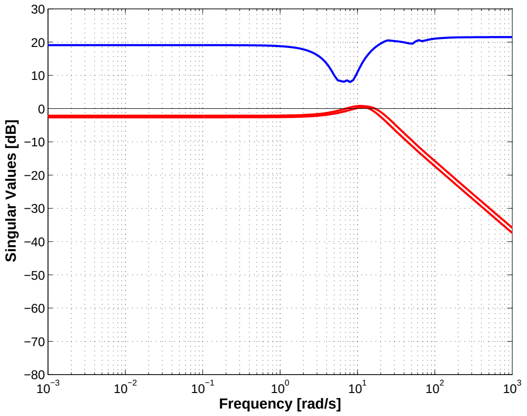

Figure 7: $C_{KF}(j\omega)$ robust stability condition.

Where K is found solving the second A.R.E. of Equation (18).

$$0 = -KA_p - A_p'K - C_p'C_p + \frac{1}{\rho}KB_{p1}B_{p1}'K \quad (18)$$

Finally, the controller transfer functions matrix $K(s)$ is described by Equation (19).

$$K(s) = G(sI - A_p + B_{p1}G + HC_p)^{-1}H \quad (19)$$

Figure 8 contains the final open-loop $G_p(s)K(s)$ system singular values plot (red lines), the target loop $G_{KF}(s)$ singular values plot (blue lines) and the robustness performance barriers (dashed blue lines), where it is clear that the final controlled systems respects the robustness performance condition.

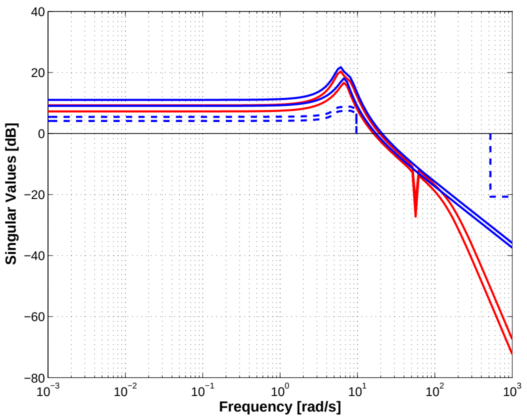

Figure 8: $G_p(s)K(s)$ and $G_{KF}(s)$ robustness performance condition.

Figure 9 presents the singular values of $[I + G_p(j\omega)K(j\omega)]^{-1}G_p(j\omega)K(j\omega)$ (red lines) and the stability condition barrier (blue line), where it is also clear that the final controlled systems respects the robust stability condition.

4 Results

Disturbance inputs, which are described by Equation (20), and the final design of $K(s)$ are applied

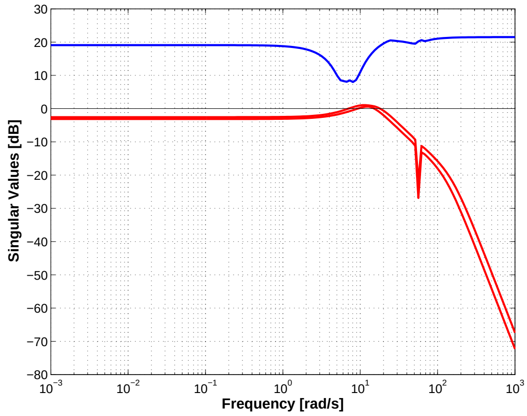

Figure 9: $C_p(s)$ robust stability condition.

into the half-vehicle model with nonlinear actuators in order to assess the designed LQG/LTR robust controller effectiveness.

$$\omega(t) = 0.038(1 - cos(8\pi t)) \quad (20)$$

Frontal bump occurs to $0.75 < t < 1.00$ and rear one to $1.50 < t < 1.75$, where t is the simulation time. The considered half-vehicle model parameters are: $M = 580kg$, $m_f = m_r = 59kg$; $I = 900kg/m^2$; $l_f = 0.90m$, $l_r = 1.25m$; $k_f = k_r = 16812N/m$, $k_{tf} = k_{tr} = 190000N/m$; $b_f = b_r = 1000N/m/s$. Active suspension system quality is evaluated according to $y(t)$ response and ride comfort improvement, whose metric is defined in Equation (21) (ISO, 1997).

$$Z_{RMS} = \sqrt{\frac{1}{N}\Sigma|Z_i|^2}, \ (1 \leq i \leq N) \quad (21)$$

Figure 10 initiates $y(t)$ analysis with $Z(t)$ profile (red line) in comparison with the half-vehicle system open-loop response (black line).

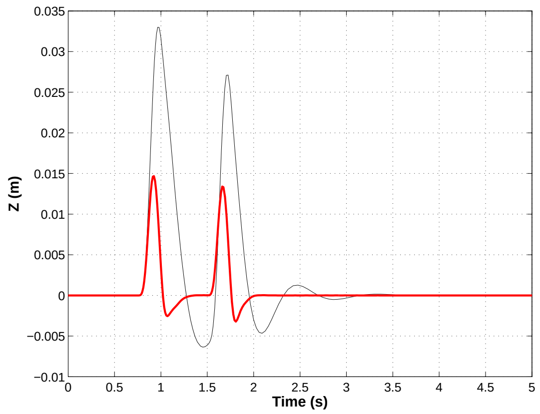

Figure 10: Chassis vertical position profile.

Active suspension system had a reduction of maximum displacement around 51% and settling time around 65% when compared with the passive system response. Both curves do not presented steady state error. The second output variable $\theta(t)$ (red line) is presented in Figure 11, together with the open-loop response (black line), where the improvements for displacement and settling time were around 53% and 69% respectively.

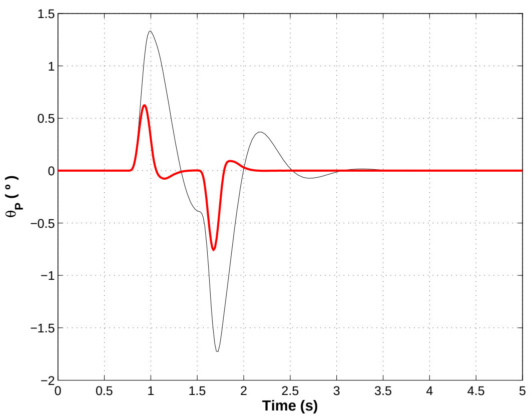

Figure 11: Chassis pitch angle profile.

Figure 12 presents rear (red line) and frontal (blue line) suspensions displacements curves whose compression and extension limits of $0.08m$ were respected.

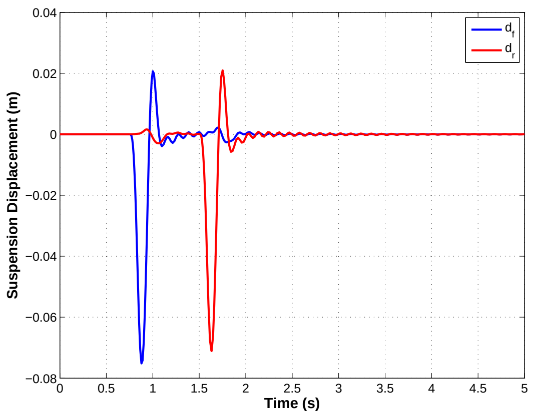

Figure 12: Suspension Displacement.

Regarding comfort metrics, the active system presented an improvement of 21.7%, with a final value 1.26 m/s^2, being considered as *uncomfortable* suspension system response. The passive system may be considered as *Very uncomfortable*, with a metric value of 1.61 m/s^2.

Simulated forces exhibited peaks of $2970N$, extrapolating model limits described in van der Sande (2011), although Root-Mean-Square force limit was respected to a maximum value of $518.49N$. To an actuator which is well defined up to $2000N$, a maximum damping force over $1100N$, which would represent $9.8A$ within linear control, states the great influence of nonlinear model portion on final system response.

5 Conclusions

This work proposed a LQG/LTR robust controller design to control an active electromagnetic suspension system applied on a half-vehicle model aiming chassis stabilization. Control parameters were selected via a numerical process due to the distortion caused by the nonlinear characteristics of the model, which were not considered into the plant, on the final system behavior. Therefore, graphical tools employed in control technique ended up being used as results analysis tools.

However, the necessary precautions were carried out and the active system, simulated with disturbance bump signals applied into the wheels, enhanced not only control variables stabilization, but also user comfort perception and settling time, whilst guaranteeing the limits of suspensions travel and RMS actuators force. Lastly, this paper performed a detailed analysis of nonlinearities influence on suspension system behavior, whose final conclusions were that damping force (nonlinear passive portion of actuators force) represents a relevant portion of final actuation force and should be considered within control systems to improve active suspension system response.

References

Alleyne, A. and Hedrick, J. K. (1995). Nonlinear adaptive control of active suspensions, *Control Systems Technology, IEEE Transactions on* **3**(1): 94–101.

Cruz, J. d. (1996). *Controle Robusto Multivariável: O Método LGQ/LTR Vol. 05*, EdUSP.

dos Santos, M. M. (2010). Controle h-infinito em suspensões ativas aplicando técnicas baseadas em desigualdades matriciais lineares.

Huang, C.-J. and Lin, J.-S. (2004). Nonlinear active suspension control design applied to a half-car model, *Networking, Sensing and Control, 2004 IEEE International Conference on*, Vol. 2, IEEE, pp. 719–724.

ISO, M. (1997). vibration and shock–evaluation of human exposure to whole body vibrations–part 1: General requirements, *ISO 2631* **1**.

Kong, Y., Zhao, D., Yang, B., Han, C. and Han, K. (2015). Robust non-fragile h-inf/ l2-l-inf control of uncertain linear system with time-delay and application to vehicle active suspension, *International Journal of Robust and Nonlinear Control* **25**(13): 2122–2141.

van der Sande, T. (2011). Control of an automotive electromagnetic suspension system, *Master's thesis, Eindhoven University of Technology* .